Ultrafast Electron Injection: Implications for a Photoelectrochemical Cell Utilizing an Anthocyanin Dye-Sensitized TiO_2 Nanocrystalline Electrode

Nerine J. Cherepy,[†] Greg P. Smestad,*[,‡] Michael Grätzel,[‡] and Jin Z. Zhang*[,†]

Department of Chemistry, University of California, Santa Cruz, Santa Cruz, California 95064, and Institute of Physical Chemistry, ICP-2, Swiss Federal Institute of Technology, CH-1015 Lausanne, Switzerland

Received: July 7, 1997; In Final Form: September 7, 1997[⊗]

A photoelectrochemical cell utilizing flavonoid anthocyanin dyes extracted from blackberries, along with colloidal TiO_2 powder, is shown to convert sunlight to electrical power at an efficiency of 0.56% under full sun. Fluorescence quenching is observed for the excited state of the TiO_2-adsorbed anthocyanin dye, cyanin, and the photocurrent spectrum correlates well with the optical absorption of the cyanin-sensitized TiO_2 nanocrystalline film. The incident photon-to-current efficiency of 19% at the peak of the visible absorption band of the dye, the open-circuit voltages of 0.5−0.4 V, and short-circuit photocurrents of 1.5−2.2 mA/cm^2 are remarkable for such a simple system and suggest efficient charge carrier injection. The ultrafast excited-state dynamics of cyanin in solution are compared with those of surface-adsorbed cyanin on TiO_2 and ZrO_2 colloids, as well as complexed with Al(III) ions. A transient absorption signal with a risetime of $<$100 fs for cyanin-sensitized TiO_2 nanoparticles is assigned to electrons injected from the dye to TiO_2. This signal is fit to a double-exponential decay with time constants of 0.52 and 67 ps. The 0.52 ps component is due to trapping of conduction band electrons or to fast direct recombination with the dye cation, while the 67 ps decay is attributed to trap state mediated indirect recombination. In contrast, stimulated emission with a 2.6 ps decay time is observed for cyanin in solution, cyanin on ZrO_2, and cyanin complexed with Al(III) ions. When compared to the photon-to-current efficiency measured for the solar cell, the efficiency estimated from the injection and recombination rate constants suggests that electron recapture by the redox mediator and light screening mechanisms may limit the efficiency of the cell.

Introduction

Electron transfer from colored dyes to wide bandgap semiconductors is of technological importance in photography as well as for photoelectrochemical energy conversion. Wide bandgap semiconductors, such as TiO_2 and AgBr, may be sensitized to visible light using surface-adsorbed dye molecules. The nanocrystalline dye-sensitized solar cell[1] is a photoelectrochemical cell inspired by the energy and electron-transfer mechanisms in natural photosynthesis and in the dye-sensitized silver halide emulsions used for photography. It parallels photosynthesis in the use of an organic dye as the light harvester to produce excited electrons, with titanium dioxide replacing carbon dioxide as the electron acceptor, iodide and triiodide replacing water and oxygen as the electron donor and oxidation product, and a multilayer structure (similar to the thylakoid membrane) to enhance both the light absorption and electron collection efficiency (Figure 1). The light-driven electrochemical process in the nanocrystalline solar cell is regenerative, and the working voltage produced by the device is the difference between the chemical potential of the titanium dioxide (Fermi level) and the redox potential of the mediator (I^-/I_3^-). Dye-sensitized nanocrystalline TiO_2 solar cells have achieved greater than 9% sunlight to electrical power conversion efficiencies and $>$16 mA/cm^2 photocurrents.[2,3] This is to be compared with 15−17% conversion efficiency for commercial silicon solar cell modules,[4,5] 1% for tropical forest ecosystems,[6] and 13% for the calculated limit for natural photosynthesis.[7]

The high solar energy conversion efficiencies of solar cells employing dye-sensitized nanocrystalline films of TiO_2[3] have spawned many recent studies of similar photoelectrochemical systems based on dye sensitization.[8−13] A detailed understanding of the mechanism and time scale of electron transfer from surface-adsorbed dyes to semiconductors will help to explain the high conversion efficiencies and to improve them further. Femtosecond laser techniques make it possible to explore the initial steps of the electron injection and recombination.[14−18]

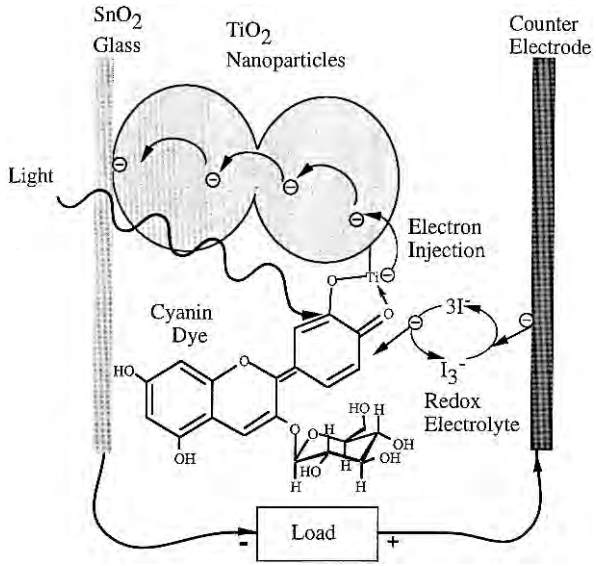

Figure 1. Dye-sensitized TiO_2 solar cell operation principle. The photoexcited dye transfers an electron to the semiconducting titanium dioxide layer via electron injection. Shown is the structure for the quinonoidal form attached to the TiO_2 surface. The electron is then transported through the rough, porous TiO_2 layer and collected by the conductive layer on the glass. Within the electrolyte, the mediator (I^-/I_3^-) undergoes oxidation (and regeneration). The electrons lost by the dye to the TiO_2 are replaced by the iodide, resulting in iodine or triiodide, which in turn obtains an electron at the catalyst-coated counter electrode as current flows through the electrical load.

[†] University of California at Santa Cruz.
[‡] Swiss Federal Institute of Technology, Lausanne.
* To whom correspondence should be addressed.
[⊗] Abstract published in *Advance ACS Abstracts,* October 15, 1997.

S1089-5647(97)02197-4 CCC: $14.00

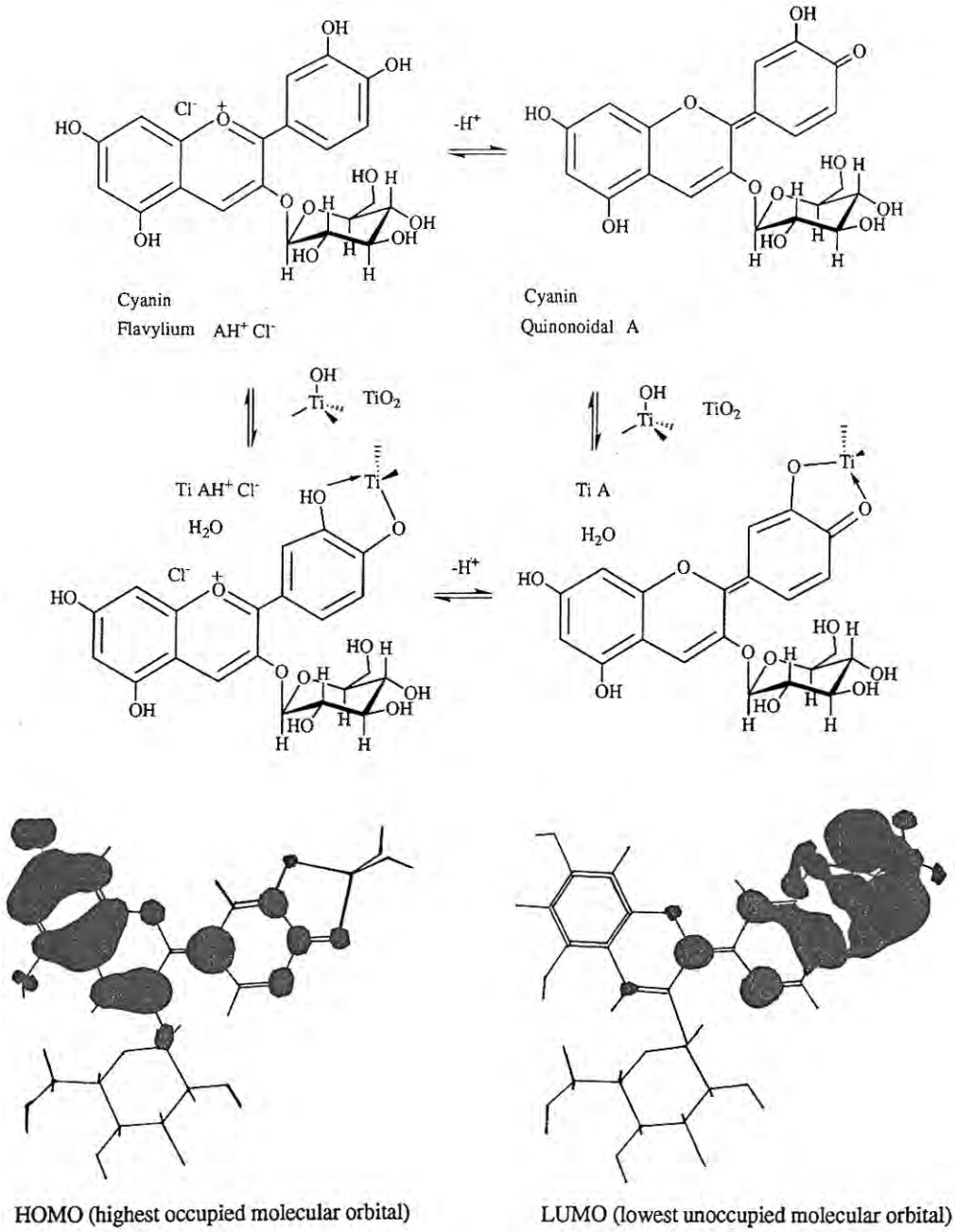

Figure 2. Schematic representation of equilibrium between the red (flavylium) and the purple (quinonoidal) forms of cyanidin 3-glucoside. At acidic pH, the dye exists mostly in the flavylium form in solution, but upon adsorption to TiO_2, the equilibrium between the adsorbed forms is thought to be shifted toward the quinonoidal form since the complexed cyanin appears purple.[28] The molecular orbital calculations of the electron density of the HOMO and LUMO of the quinonoidal form complexed with a Ti(IV) ion are also shown.

Comparison of the injection time and the recombination time measured in these experiments should allow for selection of efficient dye compounds for the nanocrystalline solar cell (or light detector). While the ruthenium-based dyes used in the nanocrystalline solar cell to attain high conversion efficiency are difficult to synthesize, we demonstrate here that readily available natural dyes can be employed to expose aspects of kinetics and energetics that determine the injection and energy conversion efficiencies.

Natural dyes, such as chlorophyll derivatives, have previously been used to sensitize TiO_2 nanocrystalline solar cells, achieving efficiencies of 2.6% and 9.4 mA/cm^2, but these dyes still require involved pigment purification and the coadsorption of other compounds on the TiO_2 surface.[19] Tennakone and co-workers have used cyanidin (cyanin without the sugar moiety) in a dye-sensitized nanocrystalline solar cell.[20] However, cyanidin is harder to isolate and less photostable than cyanin.[21]

Flavonoids are sugar-bound polyphenols found in all land plants.[22] A class of flavonoids known as anthocyanins are responsible for the red and purple colors of many fruits and flowers. The most common anthocyanin dye, cyanin, colors poppies red and cornflowers blue. A wide repertoire of colors in the red−blue range is available to anthocyanins as a result of their complexation with other polyphenols, pectins, and metal ions. While proposed biological roles of anthocyanins include insect attraction, photoprotection,[22] as endogenous antioxidants,[23] photoinhibition modulation,[24] and photosynthesis enhancement, the full scope of their abilities, as well as their photophysics, has yet to be fully characterized. Since no previous time-resolved spectroscopy of any anthocyanin pigments are available for comparison, here we report a unique set of measurements of the excited-state dynamics of cyanin.

In acidic solution, cyanin appears red and has a strong absorption band at ~520 nm. This visible absorption band is

pH and solvent sensitive, causing the dye to appear red (flavylium form) in acidic solution and purple (quinonoidal form) as pH increases, and it is deprotonated (Figure 2). The visible absorption band also shifts to the red upon complexation with metal ions, including aluminum, iron, tin, titanium, chromium, and uranium.[25−29] It is thought that the metal ions compete with the protons, displacing them and shifting the flavylium−quinonoidal equilibrium toward the quinonoidal form in a mononuclear bidentate coordination complex with metal ions. The 520 nm absorption band has also been shown to shift to the red through self-association at high concentrations ($>10^{-3}$ M) and when present in supermolecular structures involving close interactions with other flavonoids and metal ions.[26,27]

Adsorption of cyanin to the surface of TiO_2 is a rapid reaction, displacing an OH^- counterion from the Ti(IV) site that combines with a proton donated by the cyanin moiety, forming one molecule of H_2O and a very strong complex. This surface-adsorbed complex is the quinonoidal form, TiA, in equilibrium with some small amount of the flavylium form, TiA^+H (Figure 2). The complexation geometry, mononuclear bidentate, is well-known from comparison with anthocyanins which do not complex metal ions,[25] Al(III) complexation studies,[28] and a number of more recent detailed studies of adsorption to metal oxide surfaces by catechol and similar species (see for example ref 30). The adsorption geometry shown in Figure 2 is proposed as the injecting species, although there are likely other ways in which the dye may attach to the TiO_2 surface. Also shown in Figure 2 are molecular orbital calculations using the Spartan software package from Wavefunction Inc., indicating that, for the quinonoidal form complexed with Ti(IV), the HOMO (highest occupied molecular orbital) is located on the chromophore end of the complex, while the LUMO (lowest unoccupied molecular orbital) electron density is located near the Ti end.

Many studies of dye-sensitized wide bandgap semiconductors have detailed the kinetics of charge recombination (see for example refs 11 and 31−36), but it has proven difficult to measure the initial electron injection time in any of these systems. The electron injection time constants measured in earlier subpicosecond experiments on dye-sensitized wide bandgap semiconductors have mainly been reported to be less than 200 fs, although some of these results were ambiguous due to spectral overlap of the excited-state absorption of the dye and conduction band electrons in the semiconductor or were limited to measurements of the dynamics of the dye.[14−18]

An early study of an oxazine dye-sensitized SnS_2 electrode measured electron injection into the semiconductor in less than 100 fs, followed by recombination with biphasic kinetics of 10 ps and a variable component in the hundreds of picoseconds range.[14] These components were assigned to direct recombination (electron recombining at the same dye molecule from which it was injected) and indirect recombination (electron relaxation/diffusion to another recombination center or dye cation). Rehm et al.[16] reported electron injection from coumarin 343 to TiO_2 nanoparticles in less than 200 fs. Similarly, Burfeindt et al.[15] measured a temperature-independent fluorescence lifetime of 190 fs for perylene adsorbed to a TiO_2 nanocrystalline film and concomitant risetime for the perylene cation. Tachibana et al.[17] interpreted ultrafast transient absorption data of a ruthenium dye, Ru(II)(2,2′-bipyridyl-4,4′-dicarboxylate)$_2$(NCS)$_2$, adsorbed to a TiO_2 nanocrystalline film as showing biphasic electron injection with less than 150 fs and 1.2 ps components. Recombination for this system was determined by measuring the decay of the dye cation absorption, which occurred on the millisecond time scale. Another pertinent study by Martini et al.[18] of cresyl violet aggregates adsorbed electrostatically on SnO_2 found <200 fs electron injection and assigned a 12.3 ps component to direct recombination.

Here, we present the ultrafast transient decay profiles of cyanin in solution with those of cyanin adsorbed on TiO_2 colloid. These measurements allow us to determine the excited-state lifetime of the dye and the electron injection and recombination rates in the dye-sensitized TiO_2 colloid. We then correlate the energy conversion efficiency of a simple cyanin-based light detector or solar cell with measurements of the electron injection and recombination rates.

Experimental Section

Dye and Colloid Preparation. A mixture of cyanin 3-glycoside and cyanin 3-rutinoside was isolated from California blackberries (*Rubus ursinus*). These are the only anthocyanins present in blackberries. The pigments were extracted using methanol/acetic acid/water (25:4:21), and the filtered extract was passed through a Sephadex LH 20 column in the same solvent. Thirty fractions were collected, each with a volume of approximately 10 mL. Fractions 9−20 exhibited an absorbance ratio $A_{520}/A_{280} > 1$ and were used in further experiments. The flavonoid dyes quercetin and rutin were obtained from Fluka and used as supplied.

The TiO_2 and ZrO_2 colloids were prepared as described previously.[30,37] $TiCl_4$ (or $ZrCl_4$) was hydrolyzed in water at 0 °C, resulting in anatase TiO_2 (or ZrO_2) particles (average diameter 50 Å). Dye-sensitized TiO_2 and ZrO_2 colloids used in the femtosecond measurements were prepared by rapid mixing of the TiO_2 or ZrO_2 colloid with the dye to final concentrations of 4 g/L of TiO_2 or ZrO_2 and 10^{-4} M cyanin ($OD_{\lambda_{max}} = 3.5$, $\epsilon = 35\,000$ M^{-1} cm^{-1})[38] in acidic methanolic solution (pH = 3). The ZrO_2 colloid also contained trace amounts of ethanol. These solutions were diluted by a factor of 7−10 for absorption and fluorescence measurements (shown in Figure 5). For the dye-sensitized colloid used for laser experiments, out of a total OD at 390 nm of 1.00, the contribution from TiO_2 alone is 0.18. The solutions of cyanin with Al^{3+} ions were prepared by adding excess $AlCl_3$ ($\sim 10^{-2}$ M) to acidic methanolic cyanin solution.

Fabrication of Cyanin-Sensitized Solar Cell. The TiO_2 films were created from commercial colloidal TiO_2 powder (Degussa P25, average size 10−50 nm) using a simplified procedure similar to that in the literature,[2,3] except that 20 mL of an acetic or nitric acid solution (pH = 3−4 in deionized water) was ground with the powder in a mortar and pestle instead of the 20 mL of deionized water and acetylacetone. Scotch (3M) adhesive tape was applied to the two longer sides of a conductive glass plate (10−15 Ω/square Libbey Owens Ford, SnO_2:F coated) to mask a 0.5 cm strip on each edge and to form a mold or channel into which the TiO_2 solution can flow. A droplet (~ 5 $\mu L/cm^2$) of the TiO_2 solution was distributed uniformly on the plate by sliding a glass rod over the plate, and the film was allowed to dry in air. The tape was removed, and the film was annealed in an air stream at 450 °C for 30 min, cooled, and then placed in the cyanin dye solution. A drop of the electrolyte (0.5 M potassium iodide and 0.05 M iodine in water-free ethylene glycol or propylene carbonate) was placed on the stained TiO_2 film, and the counter electrode was offset laterally and placed on top. The counter electrode was prepared by distributing a drop of hexachloroplatinic acid (10 mM in 2-propanol) on the conductive side of another piece of glass and then air-annealing at 380−400 °C for 30 min. Alternatively, carbon can be deposited on the counter electrode using the graphite from a pencil to serve as the redox catalyst.

Current−Voltage and Photocurrent Action Spectra. The current voltage ($I-V$) curves were measured using a 500 Ω

potentiometer as a variable load while the cell was illuminated by a 50 W (GE 12V) tungsten halogen lamp equipped with integral parabolic reflector and UV−IR blocking filter. The lamp intensity was calibrated using an AM 1.5 Oriel solar simulator as well as measurements taken outside on a clear day in the California sunshine using a Kipp & Zonnen CM 11 pyranometer to determine the irradiance. The irradiance produced by the tungsten halogen lamp was adjusted so that the short-circuit photocurrent of test cell was identical with the value obtained using the solar simulator or sunlight. Incident photon-to-current efficiency (IPCE) measurements were performed using a tungsten halogen light source, Bausch and Lomb monochromator, and Schott RG800 (800 nm) long-wavelength pass order-sorting filter.

Optical Absorption and Fluorescence. Visible absorption spectra were taken with a Hewlett-Packard 8452A diode array spectrophotometer referenced to methanol/acetic acid/water. Fluorescence spectra were recorded on a Jobin Yvon-Spex Fluoromax 2 spectrofluorimeter, and the quantum yield of fluorescence for cyanin ($\Phi_f = 10^{-4}$) was determined by referencing to Rhodamine 6G ($\Phi_f = 0.95$).[39] The dye-loaded TiO_2 film absorptivity was obtained from transmission and reflection measurements using a Perkin-Elmer, Lambda 19 double beam spectrophotometer equipped with an integrating sphere.

Ultrafast Measurements (Excited-State Dynamics). The ultrafast transient absorption and stimulated emission measurements were obtained with a regeneratively amplified mode-locked femtosecond Ti−sapphire laser system. The laser system and experimental setup have been described previously.[40] Pulses of 40 fs duration and 5 nJ/pulse at 100 MHz were generated with a Ti−sapphire oscillator pumped with an Ar^+ laser (Coherent) and then amplified in a regenerative amplifier (Quantronix) using chirped-pulse amplification. Amplified pulses of 200 fs duration with energy of 250 μJ/pulse at 780 nm were generated at 1 kHz. This beam was frequency-doubled, resulting in 390 nm, 15 μJ pulses which were used to excite the sample. These pulses were attenuated with neutral density filters to 2−7.5 μJ/pulse. The remaining 780 nm light was used to generate a white light continuum, from which a probe pulse, e.g., 720 or 790 nm, was selected using band-pass filters (fwhm 10 nm) to probe the dye in solution, complexed with Al(III) ions, and adsorbed to ZrO_2 or TiO_2 colloid. The time delay between the pump and probe pulses (beam overlap area 1 mm^2) was controlled by a translation stage, allowing measurement of the excited-state dynamics. The kinetic data were fit with a nonlinear least-squares algorithm and Igor Pro software.

Results

I. Cyanin-Sensitized Photoelectrochemical Cell. *Current−Voltage Characteristics.* A dye-sensitized TiO_2 film can produce a significant electrical output when coupled to a counter electrode via an iodide/triiodide redox mediator and liquid electrolyte. A typical current−voltage ($I-V$) curve for an AM 1.5-illuminated (air mass 1.5, 1000 W/m^2 standard spectrum = AM 1.5)[41] cyanin-sensitized TiO_2 film, of active area 0.9 cm^2, is shown in Figure 3. A 7−10 μm thick colloidal TiO_2 film is completely stained to a dark purple color by a cyanin solution in under 5 min. The measured open-circuit voltages of cyanin-sensitized solar cells were 0.4−0.45 V, and short-circuit photocurrents were 1.5−2.2 mA/cm^2. These electrical output values are remarkable, considering the simple extraction procedure for this natural dye. From the maximum of the product of current and voltage in Figure 3, the sunlight-to-electricity conversion efficiency[4,5] was 0.56% at full sun.

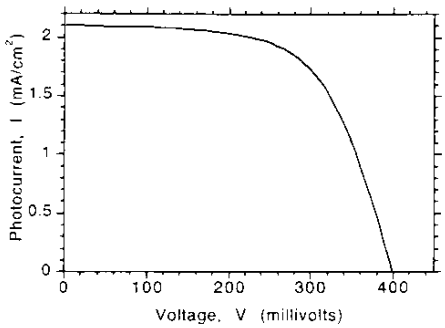

Figure 3. Current−voltage ($I-V$) curve for the illuminated cyanin-sensitized TiO_2 film. The $I-V$ curves were measured using a 500 Ω potentiometer variable load while the cell was illuminated by a 50 W (GE 12V) tungsten halogen lamp equipped with integral parabolic reflector and UV−IR blocking filter and calibrated to the AM 1.5 standard solar spectrum.

The open-circuit voltage decreased from 0.5 to 0.4 V over the first 10 min of illumination, while the photocurrent increased from 1.2 to 2 mA/cm^2 during the same period. Over the course of the next 30 min of illumination, the voltage and current slowly decreased to 0.35 V and 0.5 mA/cm^2, respectively. If a UV cutoff filter (blocking $\lambda < 400$ nm) was placed on top of the cell during illumination, this degradation was dramatically decreased, and the cell output remained constant for several hours. This suggests either photodegradation of the dye or electrolyte or a change in the effective pH of the cell. Surface-adsorbed protons are known to shift the TiO_2 Fermi level, altering the energy levels available for electron injection.[42] Devices stored for several months in a sealed container could be revived by washing the electrodes with ethanol, drying in air, reapplying the electrolyte, and reassembling the cell, resulting in only 1−2% decrease in power output compared with a new cell. Studies are currently in progress to determine the longevity of illuminated cyanin-sensitized nanocrystalline solar cells sealed with low melting point polymer films used in food packaging, such as Dupont Surlyn 1702.

A solar cell that was more UV-stable under illumination was prepared by applying the related yellow flavonoids, quercetin and rutin,[43] as coadsorbates during cyanin dye uptake. Quercetin and rutin without cyanin produced significant voltages and currents themselves (0.38 V and 0.8 mA/cm^2). It is noteworthy that significant photocurrents (1−1.2 mA/cm^2) and similar open-circuit photovoltages (0.40−0.43 V) were also obtained when the TiO_2 film was simply placed on crushed blackberries. In this case, a mixture of flavonoids attaches to the TiO_2 surface, perhaps forming a copigmentation cocktail more closely matching the in vivo condition. Juice from any plant material with high cyanin content (blackberries, raspberries, hibiscus flowers, or pomegranate seeds) also yielded similar results.

Photocurrent Action Spectrum. Figure 4 shows the incident photon-to-current efficiency (IPCE), or action spectrum, as well as the fraction of the incident light (optical absorptivity)^2 absorbed by the dye-loaded film. The IPCE at the peak of the visible absorption band (535 nm) was found to be 0.18−0.19. Integrating the product of the IPCE and the photon flux derived from the AM 1.5 standard solar spectrum[41] yields 2.3 mA/cm^2, in excellent agreement with the short-circuit photocurrent measured in Figure 3. Integrating the product of the absorptivity and the photon flux derived from the AM 1.5 solar spectrum, one obtains 12.1 mA/cm^2. Since the absorptivity determines the maximum IPCE that could be expected, this value represents the maximum possible short-circuit photocurrent for the cyanin-sensitized film illuminated by sunlight.

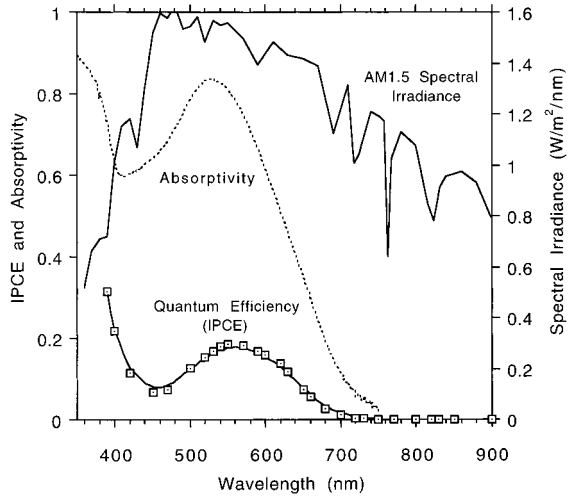

Figure 4. Photocurrent action spectrum (IPCE) for the device in Figure 3 overlaid with absorptivity spectrum of cyanin on TiO_2 nanocrystalline film and the standard solar spectrum irradiance (AM 1.5). The IPCE is the short-circuit electron flux produced by the cyanin-sensitized film divided by the incident photon flux at each wavelength. The absorptivity is the fraction of the incoming light absorbed by the cyanin-loaded TiO_2 film.

II. Cyanin-Sensitized TiO_2 Nanoparticles. *Steady-State Absorption and Fluorescence Spectra.* The absorption spectra and the fluorescence spectra of cyanin in four different environments are presented in Figure 5. Excitation at 520 nm was chosen on resonance with the lowest energy transition of cyanin. Figure 5A shows the absorption and fluorescence spectra of cyanin in solution. With 520 nm excitation, a weak fluorescence band ($\Phi_f = 10^{-4}$) peaks at 570 and extends to ~800 nm (dashed line) and is tentatively assigned to the S_1-S_0 transition. The excitation of cyanin at 390 nm produces fluorescence in the 570 nm band as well as a band peaked near 420 nm (dotted line), which is about 3 times more intense than the 570 nm band. The sharp feature at ~450 nm is the water Raman band. The probe wavelengths of 720 and 790 nm, also shown, used in the ultrafast experiments were chosen on the red edge of the S_1-S_0 emission in order to produce stimulated emission between the ground and first excited state, without possible interference from higher excited states.

The absorption and emission spectra of cyanin adsorbed to TiO_2 colloid are shown in Figure 5B. A significant shift in the absorption maximum to 532 nm and a pronounced red tail extending to 730 nm contrasts with the narrower absorption band of cyanin in solution, which does not absorb beyond ~620 nm. Even more striking is the emission spectrum from cyanin-sensitized TiO_2, which has an integrated area of about one-half the intensity of that of cyanin alone and seems to be split into two peaks, one at 550 nm and one at 740 nm. A three-point excitation profile acquired with excitation at 520, 560, and 600 nm for the emission at 740 nm is shown with the open symbols. It suggests that the species responsible for the 740 nm band absorbs more strongly in the red edge of the absorption band.

The absorption and fluorescence spectra of cyanin-sensitized ZrO_2 colloid are presented in Figure 5C. ZrO_2 has a conduction band edge 1 eV more negative than TiO_2, rendering cyanin incapable of electron injection. Also, of the metal oxides, the acid/base surface properties and refractive index of ZrO_2 most closely resemble those of TiO_2.[44] Cyanin is assumed to adsorb to both TiO_2 and ZrO_2 with the same geometry at the Ti(IV) and Zr(IV) sites. In both cases, a red shift of the absorption maximum to about 530 nm and long tail, extending to about 730 nm, is observed. A red shift in fluorescence maximum, to

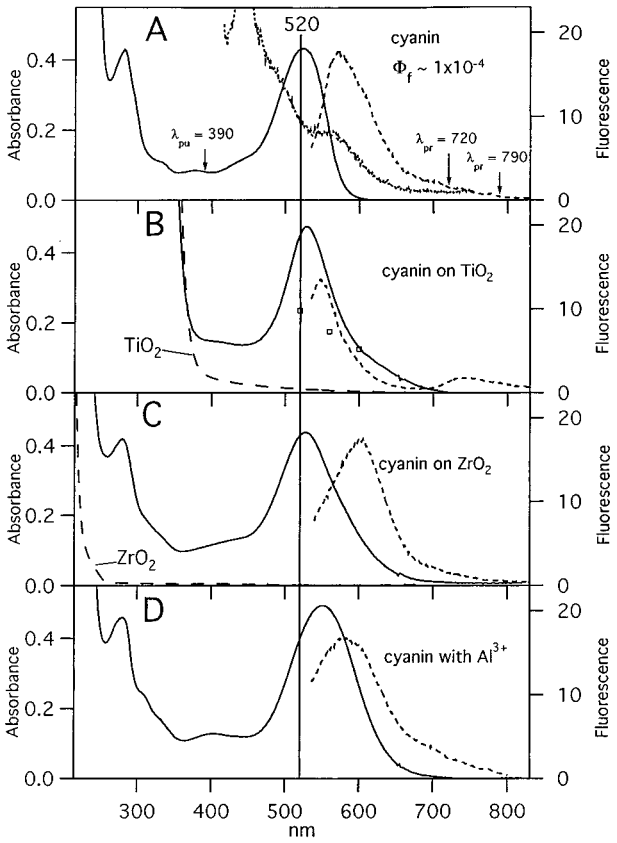

Figure 5. Absorption (—) and emission (— —) spectra excited at 520 nm of (A) 10^{-5} M cyanin in methanol/acetic acid/water (25:4:21), (B) 10^{-5} M cyanin adsorbed to 0.4 g/L TiO_2 colloid, (C) 10^{-5} M cyanin adsorbed to 0.4 g/L ZrO_2 colloid, and (D) 10^{-5} M cyanin complexed with excess Al(III) ions. The cyanin emission spectrum excited at 390 nm (---), divided by a factor of 2, is also presented in (A). The open symbols overlaid on the cyanin-sensitized TiO_2 emission spectrum (B) are a three-point excitation profile of the 740 nm emission. The pump wavelength of 390 nm and the probe wavelengths of 720 and 790 nm used in the ultrafast measurements are also shown.

about 600 nm, is observed for cyanin-sensitized ZrO_2 nanoparticles. Thus, while the electronic absorption of cyanin seems to be perturbed in a manner similar to that of cyanin adsorbed on TiO_2, its quantum yield of fluorescence is unchanged from that of cyanin in solution. We attempted to avoid aggregation between dye molecules by keeping the dye/particle ratio below 5. Centrifugation of small aliquots of the dye/TiO_2 and dye/ZrO_2 samples used resulted in a clear solution and a colored precipitate, verifying that all the dye molecules in solution were adsorbed to the colloid. Thus, none of the steady-state emission or transient features can be due to unadsorbed dye molecules.

Cyanin complexed with Al(III) ions in solution was also studied. In this case, shown in Figure 5D, the electronic structure of cyanin is modified due to the interaction with the metal ion, but no semiconductor colloid is present. With Al(III) ions, the cyanin absorption band is broadened and has its maximum at 550 nm. The emission spectrum is broad, with a peak at approximately 590 nm.

Ultrafast Dynamics. The ultrafast transient decay profiles of cyanin in solution and cyanin-sensitized TiO_2 colloid are shown in Figure 6. Parts A and B of Figure 6 show the dynamics on the 0−8.3 and 0−85 ps time scales. For cyanin in solution, stimulated emission between the ground and first excited states is observed upon excitation with the 390 nm pump pulse, probing at 720 nm. For cyanin adsorbed to TiO_2, a transient absorption signal with a pulse-width limited risetime (<100 fs) is measured, which can only be fit to a multiple-

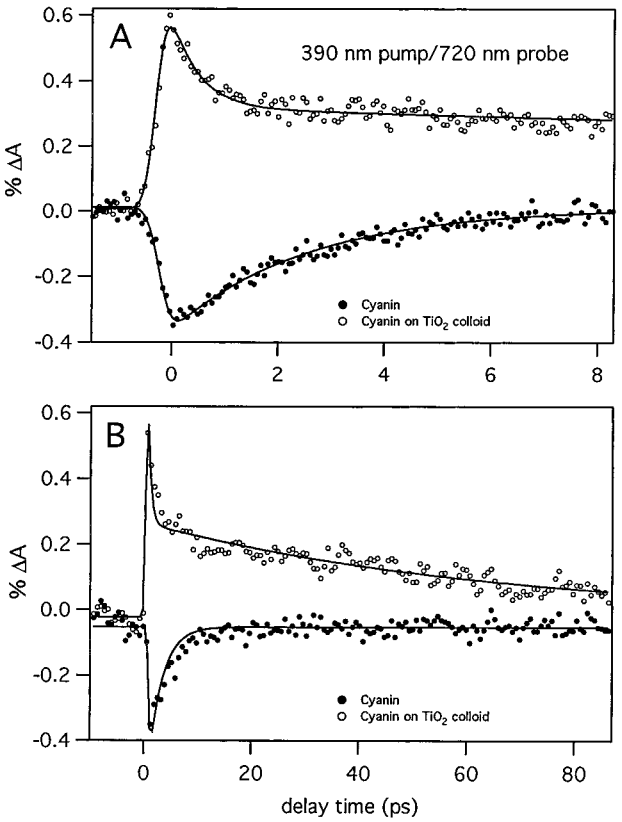

Figure 6. Experimental ultrafast stimulated emission of cyanin in solution (closed symbols) and transient absorption of cyanin-sensitized TiO_2 nanoparticles (open symbols). (A) The 0−8.3 ps window and (B) the 0−85 ps windows are fit (solid lines) simultaneously using a nonlinear least-squares fitting algorithm to a convolution of exponential decays with a Gaussian pulse representing the cross-correlation of the 390 nm pump (0.4 mJ/(pulse cm^2)) and 720 nm probe pulses. The stimulated emission from cyanin decays with a single exponential, 2.6 ± 0.7 ps, while the cyanin-sensitized TiO_2 has a transient absorption with pulse-width limited risetime, a biexponential decay with 0.52 and 67 ps components, and a small offset corresponding to persistent transient absorption which decays within ∼300 ps.

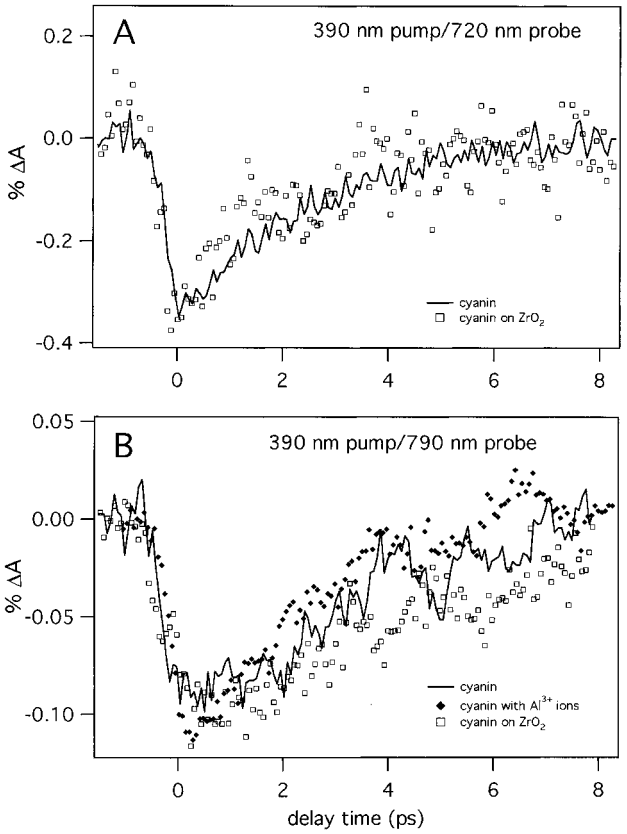

Figure 7. (A) The stimulated emission kinetics measured for 10^{-4} M cyanin in solution (solid line) and 10^{-4} M cyanin adsorbed to 4 g/L ZrO_2 colloid (open symbols) acquired with 390 nm pump (0.4 mJ/(pulse cm^2)) and 720 nm probe wavelengths. (B) The stimulated emission kinetics for cyanin in solution (solid line), cyanin adsorbed to ZrO_2 colloid (open symbols), and cyanin complexed with excess Al(III) ions (closed symbols) acquired with 390 nm pump (4 mJ/cm^2) and 790 nm probe wavelengths.

exponential decay. The solid lines are fits to the data using a convolution of exponential decays with a Gaussian pulse (fwhm = 223 fs) representing the cross-correlation of the pump and probe pulses. The stimulated emission can be fit with a single-exponential decay of 2.6 ± 0.7 ps, assigned to the lifetime of the first excited state. This short lifetime is consistent with the very weak fluorescence quantum yield measured with 520 nm excitation for cyanin ($\Phi_f = 10^{-4}$). The transient absorption observed for cyanin-sensitized TiO_2 nanoparticles was fit to two exponentials. The time constants found for the best fit are $\tau_1 = 0.52$ ps and $\tau_2 = 67$ ps with uncertainties of ∼10%. A small positive offset is necessary for the simultaneous fit to the three time windows measured (0−8.3, 0−85, and 0−600 ps), corresponding to a weak absorption signal that persists to ∼300 ps in the 0−600 ps window (not shown).

Assignment of the transient absorption signal in Figure 6 to a charge-separated cyanin$^+$$TiO_2^-$ species is supported by a comparison with the transient decay profile, shown in Figure 7, of cyanin-sensitized ZrO_2 colloid. Figure 7A shows almost identical dynamics for the stimulated emission decays of cyanin in solution and cyanin adsorbed on ZrO_2 colloid acquired with 390 nm pump and 720 nm probe wavelengths. In addition, Figure 7B shows that stimulated emission with the same ∼3 ps decay is observed for cyanin complexed with Al(III) ion, along with cyanin adsorbed to ZrO_2 colloid using 790 nm probe wavelength. A comparison of Figures 7A and 8B shows that the signal becomes weaker as the probe wavelength is tuned further off the main emission band. Thus, the free dye (flavylium form) and the metal-complexed (quinonoidal form) dye show the same excited-state decay dynamics. The decay dynamics are perturbed neither for cyanin on ZrO_2, to which the dye cannot inject electrons, nor with Al(III) ions. In contrast, instead of stimulated emission, a strong transient absorption signal is observed for cyanin-sensitized TiO_2 colloid.

The wavelength dependence of the transient absorption signal observed for cyanin adsorbed on TiO_2 colloid was studied by varying the probe wavelength between 720 and 790 nm. While the signal at 720 nm is somewhat stronger than the signal at 790 nm (see Figure 8), the kinetics appear unchanged. There also appears to be no dependence of the dynamics on pump power, as shown in Figure 9. In the range from 0.2 to 0.75 mJ/(pulse cm^2) there are no significant differences in the transient decay profile.

Discussion

The comprehensive study presented here of the use of a natural flavonoid dye, cyanin, to sensitize TiO_2 to visible light provides insight into interplay between energetics and kinetics in the dye-sensitized nanocrystalline solar cell. A number of questions have been raised by our results, including the following: (1) How does the nature of the adsorption of the dye to the TiO_2 affect efficiency? (2) What can be gleaned about the biological functionality of the anthocyanins from the excited-state dynamics of cyanin? (3) How can we unambigu-

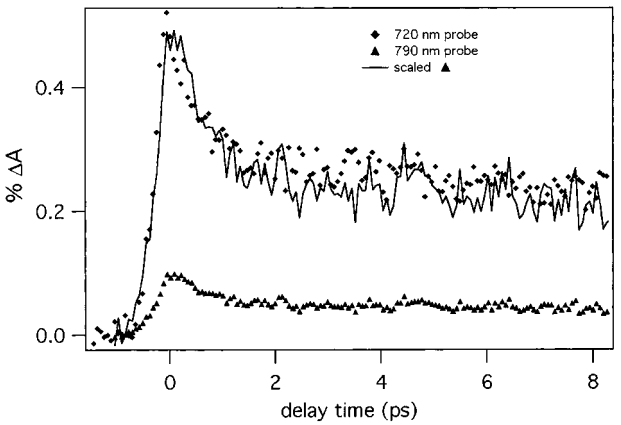

Figure 8. Wavelength dependence of the dynamics of electron injection in cyanin-sensitized TiO_2 nanoparticles. Risetime (pulse width limited) and decay kinetics for traces acquired with 720 nm probe (diamonds) and 790 nm (triangles) are in good agreement, shown by the scaled 790 nm trace (solid line) overlaying the 720 nm trace nearly exactly.

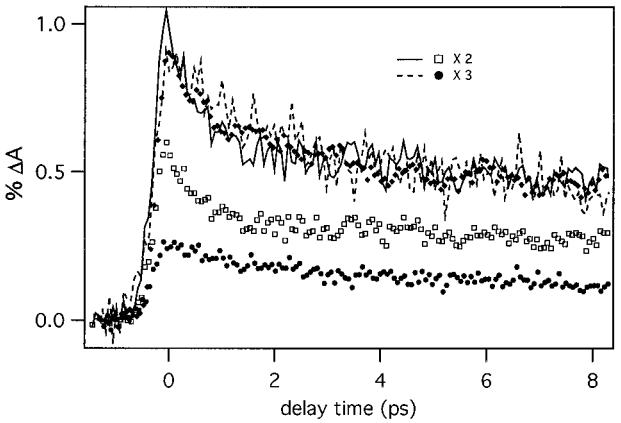

Figure 9. Power dependence of the photogenerated electrons is linear between 0.25 and 0.75 mJ/(pulse cm^2) (0.08−0.3 photons/particle). Decay kinetics acquired at 0.25 mJ/(pulse cm^2) (closed circles), 0.4 mJ/(pulse cm^2) (open squares), and 0.75 mJ/(pulse cm^2) (closed diamonds) are in good agreement as demonstrated by the scaled 0.4 mJ/(pulse cm^2) trace (solid line) and the scaled 0.25 mJ/(pulse cm^2) trace (dashed line).

ously assign the transient absorption observed for cyanin-sensitized TiO_2 nanoparticles? (4) What are the physical processes measured in the decay dynamics of cyanin-sensitized TiO_2 nanoparticles? (5) How can the kinetic measurements of the dye-sensitized colloid be used as feedback to understand limitations on the efficiency of the solar cell? We have investigated this range of issues, and we discuss here our current understanding of them and how they are interrelated.

Electronic Interaction between Cyanin and TiO_2. Adsorption of cyanin on TiO_2, detailed schematically in Figure 2, results in a mononuclear bidentate complex between the quinonoidal form of cyanin and Ti(IV) surface defects. The absorption and emission spectra of cyanin alone and complexed with both TiO_2 and ZrO_2 nanoparticles and Al(III) ions, shown in Figure 5, provide crucial information on nature of the complexation. While the absorption spectra of metal-complexed cyanin seem to be perturbed in a similar fashion with titanium, zirconium, and aluminum, the emission spectrum of cyanin adsorbed to TiO_2 differs markedly in that it appears to split into two bands. These two bands may result from subpopulations of cyanin, adsorbed in such a way that electron injection is inefficient, for example, due to interaction between dye molecules or adsorption in configurations other than mononuclear bidentate. We suggest that all the emission from cyanin adsorbed to TiO_2 in the 580−710 nm range is quenched due to electron injection; however, features at 550 and 740 nm represent subpopulations of adsorbed dye molecules that do not efficiently inject electrons to TiO_2 and may therefore exhibit fluorescence.

Preliminary molecular orbital calculations using the Spartan software package (http://www.wavefun.com/) indicate that, for the quinonoidal form complexed with the bare Ti(IV) ion, the LUMO (lowest unoccupied molecular orbital) electron density is located near the Ti end of the complex and the HOMO (highest occupied molecular orbital) is located on the opposite end (a configuration favorable for injection). Conversely, for the complexed flavylium form, the opposite orientations of the excited- and ground-state electron probability functions are calculated. These calculations contain no configuration interaction and are based on semiempirical methods and geometry-optimized structures. This asymmetry between the ground and excited state suggests the presence of charge-transfer character in the excited state of cyanin adsorbed on TiO_2 and may help to explain the ultrafast electron injection. This description of the electronic structure must be reconciled with the red-shifted absorption of cyanin on ZrO_2, yet the absence of electron injection. Conceptually, the charge-transfer state exists for both cyanin/TiO_2 and cyanin/ZrO_2, but coupling of the charge-transfer state to the conduction band is energetically allowed only for cyanin/TiO_2. Thus, strong mixing with a charge-transfer state is present for metal-complexed cyanin in all cases (Figure 5B−D), but mixing with this state provides coupling to the conduction band only for TiO_2.

Dynamics of Cyanin in Solution. The stimulated emission observed in the 720−790 nm range decays with a ∼3 ps single exponential. This decay most likely corresponds to the lifetime of the first excited state of cyanin. The fluorescence excited at 390 nm includes the 570 nm fluorescence band, but a broad emission band centered at 420 nm is observed as well (see Figure 5A). The absorption spectrum indicates that other states may contribute to the absorption at 390 nm, e.g., S_2. However, since 390 nm lies between the strong S_0-S_1 and the higher absorption bands, we propose that this excitation wavelength results in some vibrationally excited population in the S_1 state along with some population in the S_2 state. The measured strong fluorescence for the S_2 state (with 340 nm excitation the ∼420 nm band is about 500 times more intense than the 570 nm band) suggests that it should have a relatively long lifetime. The observed short lifetime in the stimulated emission is then not likely due to S_2-S_0 stimulated emission. Further work with tunable excitation is necessary to make a conclusive assignment. To ensure that the dynamics being probed were those of the first excited state, the probe wavelength was tuned to the red edge of the S_1-S_0 emission band (720−790 nm). The stimulated emission risetime is faster than the resolution of our laser system, corresponding to a majority population in the excited state within 100 fs, and it decays in ∼3 ps, suggesting that nonradiative relaxation routes dominate for the S_1-S_0 relaxation in cyanin. This rapid depopulation of the excited state of cyanin narrows the time window in which electron injection must occur in order to produce the sizable photocurrents observed in the cyanin-sensitized nanocrystalline TiO_2 photoelectrochemical solar cell.

The short lifetime of the first excited state of cyanin is consistent with its photostability and may be implicated in its role in photoprotection.[22] In vivo, cyanin would provide strong absorptivity followed by fast recovery to the ground state, allowing it to protect from light in the UV to visible range with quick turnover time. More detailed studies of flavonoid

photophysics will undoubtedly lead to better understanding of their roles in plants.

The Transient Absorption Signal for Cyanin-Sensitized TiO_2 Nanoparticles. We have measured a transient absorption signal for cyanin-sensitized TiO_2 nanoparticles with 390 nm pump and 720−790 nm probe wavelengths. The transient absorption signal is clearly a signature of charge separation, since it is observed only for cyanin adsorbed to TiO_2 and not for cyanin−ZrO_2 or cyanin−Al(III). A priori, this transient absorption may arise either from electrons in the conduction band of TiO_2, from the oxidized dye, or from a combination of these two species.

Since the quinonoidal, TiA, form of cyanin is formed upon complexation with metal ions (Figure 2),[28,29] the cation of the surface-adsorbed dye would be similar to the $TiAH^+$ or Ti-complexed flavylium form. It would be better described as TiA^+, charged but not protonated, which probably has an absorption spectrum similar to that of the AH^+, flavylium form shown in Figure 5A. From this absorption spectrum, which shows no appreciable absorption beyond 600 nm, we exclude the TiA^+ species as the origin of the transient absorption measured at 720−790 nm. We have therefore assigned the transient absorption to excited electrons in the TiO_2 particles and not to the dye cation. Regardless of this assignment, the conclusions about charge injection and recombination will not change, since the transient absorption is unequivocally due to a cyanin$^+$$TiO_2^-$ charge-separated state.

Photoexcited TiO_2 nanoparticles are known to absorb in the 500−800 nm region.[45−47] However, in the dye-sensitized TiO_2 nanoparticles, photoexcitation results only in excited electrons in TiO_2, not electron−hole pairs as in studies of bare TiO_2 nanoparticles. Nevertheless, since it has been claimed that the red edge of this absorption is due to the excited electron, it is reasonable to assign the transient absorption we measured in the 720−790 nm range to excited electrons in TiO_2. In the case of dye-sensitized particles, the electrons will be free of interactions with holes within the semiconductor particle (excitons are not generated) and are likely to follow different decay routes from photogenerated electron−hole pairs. We see no transient absorption at 720 nm from bare TiO_2 colloid of the same concentration as used for the dye-sensitized TiO_2 samples. Thus, we conclude that direct excitation of TiO_2 colloid has negligible contribution to the observed transient absorption.

As shown in Figure 9, the transient absorption profile for cyanin-sensitized TiO_2 is independent of the power of the pump pulse. Even at the maximum power employed, the fraction of cyanin molecules excited per pulse was 0.07.[48] At the concentrations employed (10^{-4} M cyanin and 4 g/L TiO_2), there are 3−4 cyanin molecules per TiO_2 particle (assuming the average particle diameter is 50 Å). It is therefore unlikely under the conditions studied that more than one electron is injected per particle. These sample conditions preclude any concerns about electron−electron interactions in the decay mechanisms for the transient absorption. The dynamics measured are in the linear regime both with respect to the sensitizing dye (low fraction excited) and with respect to generation of electrons within each particle since there is a low probability of more than one injected electron per particle.

There are several possible assignments of the 0.52 and 67 ps decay components. The following processes are expected to occur upon photoexcitation of cyanin-sensitized TiO_2 nanoparticles: (1) electron injection to the conduction band, (2) electron migration to the particle surface and electron trapping, and (3) electron recombination with the dye cation. From the data, we can assume that injection is fully developed by 100 fs, and electron migration to the surface should occur in less than 3 ps for ∼50 Å particles (based on the random walk model).[9,46] Thus, it is possible that electrons are already in shallow traps within the laser pulse, as reported for bare TiO_2 particles.[47] Alternatively, electron migration to the surface and trapping may be resolved in the transient absorption profile. Thus, the measured 0.52 ps decay component may correspond either to trapping to a shallow trap or to direct recombination facilitated by the Coulombic attraction to the nearby dye cation. The longer time component, 67 ps, may be assigned to indirect recombination mediated by trap states in TiO_2. A small offset persists on the hundreds of picoseconds time scale, showing that some excited electrons are long-lived, mostly likely in deep trap states.

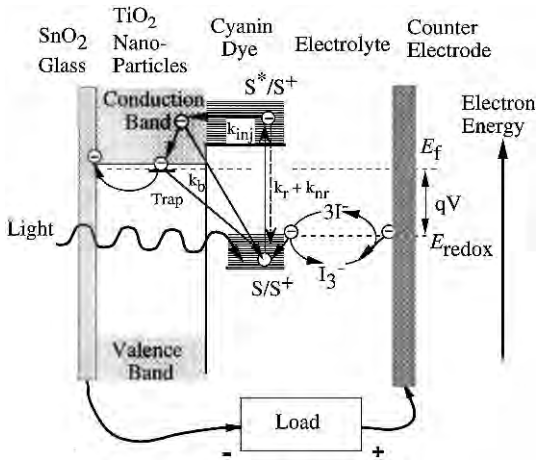

Figure 10. Schematic of the kinetics and energetics of the dye-sensitized TiO_2 nanocrystalline solar cell. Upon excitation of the dye, electron injection to the conduction band of TiO_2 occurs in competition with other excited-state decay processes of the dye, denoted by k_r and k_{nr}. The injected electron then may recombine with the dye cation (k_b), either directly or mediated by trap states, or it may hop to another TiO_2 particle in the film, migrating toward the external circuit. In the absence of recombination, iodide will reduce the dye cation.

Relationships between Dynamics and Cell Efficiency. In the quest to improve photon-to-current efficiency in the dye-sensitized solar cell, several characteristics must be optimized. First, solar absorptivity of the dye-sensitized nanocrystalline film should be strong. Second, injection should be efficient. That is, the sensitizing dye must inject electrons quickly, with few competing excited-state decay processes, so that injection is the preferred deexcitation route. Third, recombination and recapture of injected electrons before they can be collected at the back contact must be slow. An illustration of the energetics and kinetics of the cell is presented in Figure 10.

The photocurrent of the cell is determined by the photocurrent efficiency, IPCE. The IPCE at a particular excitation wavelength, λ, is the product of the absorptivity, $a(\lambda)$, injection efficiency, Φ_{inj}, and collection efficiency, Φ_c

$$\mathrm{IPCE}(\lambda) = a(\lambda)\Phi_{inj}\Phi_c \qquad (1)$$

From the absorptivity of the cyanin-sensitized film shown in Figure 4, the maximum value of $a(\lambda)$ is 0.85. From the risetime (<100 fs) of the transient absorption signal for the cyanin-sensitized TiO_2 colloid, k_{inj} is estimated to be $\sim 10^{13}$ s^{-1}. The measured decay time of the excited state, τ, of the unattached dye of 2.6 ps along with the fluorescence quantum yield, Φ_f, of 10^{-4} can be used to determine the radiative and nonradiative rate constants, k_r and k_{nr}

$$\Phi_f = \tau k_r = k_r/(k_r + k_{nr}) \qquad (2)$$

The radiative rate constant is calculated as $3.85 \times 10^7\ s^{-1}$, and the nonradiative rate constant is $3.85 \times 10^{11}\ s^{-1}$. Since the injection efficiency is given by

$$\Phi_{inj} = k_{inj}/(k_{inj} + k_r + k_{nr}) \quad (3)$$

ϕ_{inj} is calculated as 0.98. (Note that this value applies only to dye molecules that inject; some molecules are adsorbed but do not inject, as seen by the residual fluorescence for cyanin-sensitized TiO_2 nanoparticles.) Thus, if a cyanin-sensitized nanocrystalline cell could provide collection efficiency of unity, eq 1 would predict a maximum IPCE of 0.83.

After electrons have been injected into the conduction band of the TiO_2, the collection efficiency, Φ_c, determines whether they will reach the external circuit. Recombination of excited electrons with the (oxidized) dye cation can occur, as well as recapture by the oxidized redox mediator (triiodide). Recombination with the dye cation may be described by a back-electron-transfer constant, k_b. The decay of injected electrons in cyanin-sensitized TiO_2 is clearly multiexponential, but as a conservative estimate, if the 0.52 ps component is the limiting recombination decay route, we can estimate k_b as $1.9 \times 10^{12}\ s^{-1}$. The losses due to electron recapture by the triiodide are only recently being measured experimentally and may involve multiple steps including trapping and interactions at the surface between trap sites and triiodide.[10,49]

In Figure 4, we measure a maximum IPCE in the visible absorption band of 0.19. Thus, the overall efficiency must be decreased due to poor collection efficiency. If we include in eq 1 all the known rate constants affecting efficiency, we have

$$\mathrm{IPCE}(\lambda_{max}) = (a(\lambda_{max})k_{inj})/(k_{inj} + k_r + k_{nr} + k_b) \quad (4)$$

Equation 4 yields a value of 0.69. The fact that the cell maximum photon-to-current efficiency is only 0.19 suggests that recapture mechanisms may undermine the cell efficiency. Many processes control the recapture rate and may ultimately prove to limit the efficiency of the cell, rather than the initial injection rate constant.[10,49]

While the injection efficiency for the cell is calculated based on the femtosecond pump−probe measurement (390 nm excitation), we are assuming the same injection rate for excitation at the visible absorption maximum (~530 nm) of the dye. However, with 390 nm excitation, the dye is prepared highly vibrationally excited in the S_1 state, and the measured injection time (<100 fs) is faster than typical vibrational relaxation times. Thus, there is a possibility that injected electrons originating from vibrationally excited states may behave as "hot electrons", which may be more efficient than thermalized electrons.[50] Although we cannot rule out this possibility, the IPCE (Figure 4) for the cyanin-sensitized film tracks its absorptivity, rather than increasing as excitation is tuned higher in the excited-state manifold. Thus, we see no evidence for a strong wavelength dependence of the injection rate.

A possible further complication may be dye aggregation on the nanocrystalline film producing absorptivity which does not inject electrons. An important direction for future research on dye-sensitized nanocrystalline photoelectrochemical cells would be characterization of the loss of carriers due to electron recapture by the electrolyte as the electrons drift through the film to the back contact. Since these losses would appear to be constant for a particular cell fabrication procedure, yet efficiency is not as high for the cyanin-sensitized cell prepared in exactly the same way with a Ru-based dye-sensitized film, there may be dye-specific issues relating to dye surface coverage. If so, coadsorbates could be employed to improve the efficiency of the cyanin-sensitized electrode to block surface trap sites and impede triiodide contact with the TiO_2 surface as well as inhibiting dye aggregation.

Conclusions

An anthocyanin dye, cyanin, can be used to sensitize TiO_2 to visible light, providing a very simple method to study dye sensitization of semiconductors. A transient absorption signal (<100 fs rise followed by multiple exponential decay) measured for cyanin-sensitized TiO_2 nanoparticles is assigned to electrons injected from the dye into the semiconductor. This assignment is corroborated by the quenching of dye fluorescence upon adsorption and the close match between the photocurrent action spectrum and the optical absorption of the cyanin-sensitized TiO_2 nanocrystalline film. The observation of pulse-width limited (<100 fs) electron injection indicates that strong coupling via a charge-transfer interaction between cyanin and the Ti(IV) sites, where they are adsorbed, provides a conduit through which electronic excitation of the dye produces conduction band electrons in TiO_2. Although cyanin injects electrons to TiO_2 very efficiently and recombination losses with the oxidized dye are at least 1 order of magnitude slower than injection, the cell efficiency (IPCE) is only ~20% at its maximum. The losses in photocurrent efficiency may be due to (1) increased dye aggregation on the films not measured in the dynamics of cyanin-sensitized TiO_2 nanoparticles or (2) electron recapture by the electrolyte mediator, possibly involving intermediate trapping steps. The fast excited-state decay measured for cyanin in solution (2.6 ps) bolsters the conventional classification of anthocyanins as photoprotection pigments and contributes to the understanding of flavonoid photoprocesses in biological systems. The ready availability, stability, and satisfactory injection efficiency of these dyes may facilitate research and allow expansion of the principles of the dye-sensitized nanocrystalline solar cell.

Acknowledgment. N.J.C. and J.Z.Z. thank the University of California Energy Institute, the American Chemical Society Petroleum Research Fund, and the University of California at Santa Cruz for support. We are grateful to Jacques Moser for the generous gift of the TiO_2 and ZrO_2 colloids. Peter Pechy and Jacques Moser helped to elucidate the nature of the attachment (and structure) of the cyanin dye. Thanks to Robin Humphry-Baker for providing calculations of the HOMO and LUMO of the cyanin dye on TiO_2.

References and Notes

(1) O'Regan, B.; Grätzel, M. *Nature* **1991**, *353*, 737.
(2) Smestad, G.; Bignozzi, C.; Argazzi, R. *Sol. Energy Mater. Sol. Cells* **1994**, *32*, 259.
(3) Nazeeruddin, M. K.; Kay, A.; Rodicio, I.; Humphry-Baker, R.; Müller, E.; Liska, P.; Vlachopoulos, N.; Grätzel, M. *J. Am. Chem. Soc.* **1993**, *115*, 6382.
(4) Zweibel, K. *Am. Sci.* **1993**, *81*, 362.
(5) Zweibel, K. In *Harnessing Solar Power*; Plenum: New York, 1990; p 101.
(6) Smil, V. In *General Energetics, Energy in the Biosphere and Civilization*; Wiley: New York, 1992; p 53.
(7) Bolton, J. R.; Hall, D. O. *Photochem. Photobiol.* **1991**, *53*, 545.
(8) Bechinger, C.; Ferrere, S.; Zaban, A.; Sprague, J.; Gregg, B. *Nature* **1996**, *383*, 608.
(9) Hagfeldt, A.; Grätzel, M. *Chem. Rev.* **1995**, *95*, 49.
(10) Huang, S. Y.; Schlichthörl, G.; Grätzel, M.; Frank, A. J. *J. Phys. Chem. B* **1997**, *101*, 2576.
(11) Argazzi, R.; Bignozzi, C.; Heimer, T.; Castellano, F.; Meyer, G. *Inorg. Chem.* **1994**, *33*, 5741.
(12) Cao, F.; Oskam, G.; Searson, P.; Stipkala, J. M.; Heimer, T. A.; Farzad, F.; Meyer, G. J. *J. Phys. Chem.* **1995**, *99*, 17071.

(13) Matsumoto, M.; Miyazaki, H.; Matsuhiro, K.; Kumashiro, Y.; Takaoka, Y. *Solid State Ionics* **1996**, *89*, 263.
(14) Lanzafame, J. M.; Miller, R. J. D.; Muenter, A. A.; Parkinson, B. A. *J. Phys. Chem.* **1992**, *96*, 2820.
(15) Burfeindt, B.; Hannappel, T.; Storck, W.; Willig, F. *J. Phys. Chem.* **1996**, *100*, 16463.
(16) Rehm, J. M.; McLendon, G. L.; Nagasawa, Y.; Yoshihara, K.; Grätzel, M. *J. Phys. Chem.* **1996**, *100*, 9577.
(17) Tachibana, Y.; Moser, J. E.; Grätzel, M.; Klug, D. R.; Durrant, J. R. *J. Phys. Chem.* **1996**, *100*, 20056.
(18) Martini, I.; Hartland, G. V.; Kamat, P. V. *J. Phys. Chem.*, **1997**, in press.
(19) Kay, A.; Grätzel, M. *J. Phys. Chem.* **1993**, *97*, 6272.
(20) Tennakone, K.; Kumara, G. R.; Kumarasinghe, A.; Wijayantha, K.; Sirimanne, P. *Semicond. Sci. Technol.* **1995**, *10*, 1689.
(21) Tennakone, K.; Kumara, G. R.; Kottegoda, I. R.; Wijayantha, K. *Semicond. Sci. Technol.* **1997**, *12*, 128.
(22) Martin, H.-D. *Chimia* **1995**, *49*, 45.
(23) Yamasaki, H.; Uefuji, H.; Sakihama, Y. *Arch. Biochem. Biophys.* **1996**, *332*, 183.
(24) Gould, K. S.; Kuhn, D.; Lee, D.; Oberbauer, S. *Nature* **1995**, *378*, 241.
(25) Harborne, J. B. In *Comparative Biochemistry of the Flavonoids*; Academic Press: London, 1967; p 1.
(26) Bayer, E.; Egeter, H.; Fink, A.; Nether, K.; Wegmann, K. *Angew. Chem., Int. Ed. Engl.* **1966**, *5*, 791.
(27) Goto, T.; Kondo, T. *Angew. Chem., Int. Ed. Engl.* **1991**, *30*, 17.
(28) Dangles, O.; Elhabiri, M.; Brouillard, R. *J. Chem. Soc., Perkin Trans. 2* **1994**, 2587.
(29) Figueiredo, P.; Elhabiri, M.; Saito, N.; Brouillard, R. *J. Am. Chem. Soc.* **1996**, *118*, 4788.
(30) Connor, P. A.; Dobson, K. D.; McQuillan, A. J. *Langmuir* **1995**, *11*, 4193.
(31) Liu, D.; Fessenden, R.; Hug, G.; Kamat, P. *J. Phys. Chem. B* **1997**, *101*, 2583.
(32) Kamat, P. V. *Chem. Rev.* **1993**, *93*, 267.
(33) Kamat, P. V.; Das, S.; Thomas, K. G.; George, M. V. *Chem. Phys. Lett.* **1991**, *178*, 75.
(34) Moser, J.; Grätzel, M. *Chem. Phys.* **1993**, *176*, 493.
(35) Moser, J.; Grätzel, M. *J. Am. Chem. Soc.* **1984**, *106*, 6557.
(36) Arbour, N. C.; Sharma, D. K.; Langford, C. H. *J. Phys. Chem.* **1990**, *94*, 331.
(37) Moser, J.; Grätzel, M. *J. Am. Chem. Soc.* **1983**, *105*, 6547.
(38) Brouillard, R.; El Hage Chahine, J.-M. *J. Am. Chem. Soc.* **1980**, *102*, 5375.
(39) Nasr, C.; Liu, D.; Hotchandani, S.; Kamat, P. V. *J. Phys. Chem.* **1996**, *100*, 11054.
(40) Zhang, J. Z.; O'Neil, R. H.; Roberti, T. W. *J. Phys. Chem.* **1994**, *98*, 3859.
(41) *Standard for Terrestrial Solar Spectrum Irradiance Tables at Air Mass 1.5 for a 37° Tilted Surface*, ASTM Standard E892, American Society for Testing and Materials, Philadelphia, PA, 1992, 12.02.
(42) Pelizzetti, E.; Visca, M. In *Energy Resources through Photochemistry and Catalysis*; Graetzel, M., Ed.; Acedemic Press: New York, 1983; p 261.
(43) Harborne, J. B. In *Comparative Biochemistry of the Flavonoids*; Academic Press: London, 1967; p 37.
(44) Kay, A.; Humphry-Baker, R.; Grätzel, M. *J. Phys. Chem.* **1994**, *98*, 952.
(45) Rothenberger, G.; Moser, J.; Grätzel, M.; Serpone, N.; Sharma, D. K. *J. Am. Chem. Soc.* **1985**, *107*, 8054.
(46) Serpone, N.; Lawless, D.; Khairutdinov, R.; Pelizzetti, E. *J. Phys. Chem.* **1995**, *99*, 16655.
(47) Colombo, D. P.; Roussel, K. A.; Saeh, J.; Skinner, D. E.; Cavaleri, J. J.; Bowman, R. M. *Chem. Phys. Lett.* **1995**, *232*, 207.
(48) For the photon flux, $P = 4 \times 10^{12}-1.5 \times 10^{13}$ photons/pulse, focal area, $a = 1$ mm^2, and absorption cross section of cyanin adsorbed on TiO_2 at 390 nm, $\sigma_A \sim 0.45$ Å^2, we can estimate the fraction, F, of cyanin molecules excited by each pump pulse as $F = \sigma_A P/a$ to be 0.02−0.07.
(49) Stanley, A.; Matthews, D. *Aust. J. Chem.* **1995**, *48*, 1293.
(50) Ross, R. T.; Nozik, A. J. *J. Appl. Phys.* **1982**, *53*, 3813.